Energy Equip. Sys./ Vol. 11/No. 1/March 2023/ 43-53

ENERGY EQUIPSYS

Energy Equipment and Systems

http://energyequipsys.ut.ac.ir
www.energyequipsys.com

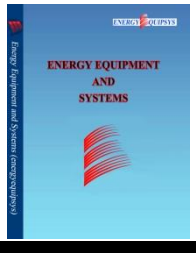

Fluid-solid interaction analysis of cantilever plate behind a fixed cylinder in parallel flow: Application to energy harvesters

Authors

Reza Roohi[a*]
Masoud Akbari [a]
Ali karimzadeh [a]

[a] Department of Mechanical Engineering, College of Engineering, Fasa University, Fasa, Iran

Article history:

Received : 21 July 2022
Accepted : 12 September 2022

ABSTRACT

In the present study, the transient vibration of a fixed cylinder attached to an elastic piezoelectric splitter plate is examined. The vibration frequency of these systems is a combination of vortex shedding frequency and splitter plate natural frequency. Therefore, Geometric plate and fluid flow parameters that affect the structure's frequency and dynamic behavior are investigated. The fluid-solid interaction model is developed for the described problem to determine the splitter motion patterns and their effect on the vortex shedding frequency and the estimated piezoelectric output power. The effect of involving parameters such as inlet fluid velocity, density ratio, splitter plate length and stiffness on the dynamic response of the device and the produced power is inspected. A comparison between the data of the present study and those reported in the literature is conducted and great agreement is achieved. Results show that the decreasing of dimensionless Young modulus of plate or increasing dimensionless plate length and density ratio decreases the natural frequency of the system. By increasing the fluid velocity from 1 to 4, 8 and 16, respectively the excitation modes of 1st, 1st and 2nd, first three and first four are activated and higher plate deflections are obtained.

Keywords: Vortex-Induced Vibration, Piezoelectric Flexible Splitter Plate, Fluid-Solid Interaction, CFD.

1. Introduction

Renewable energy harvesting has gained interest substantially by researchers recently due to several beneficial aspects [1, 2]. Wind and hydropower energy sources can be named as two conventional types of renewable energy forms which are utilized using various types of apertures [3, 4]. Among these apertures, the devices which work based on the vortex shedding behind a bluff body due to their lower cost, deployment, and installation cost as well as the minor impact on the environment are expected to have a bright future [5]. The most commonly designed and manufactured VIV energy harvesters are made of a deformable structure immersed in a fluid flow and the power is extracted from the induced vibration [6]. The effect of deformable structure's vibration on the modification of vortex shedding and coupled fluid-solid behavior of the systems are quite unknown and gaining attention in recent years [7, 8].

The flow-induced vibration (FIV) [9] and vortex-induced vibration (VIV) devices are made of a cylinder and a rigid or deformable

* Corresponding author: Reza Roohi
Department of Mechanical Engineering, College of Engineering, Fasa University, Fasa, Iran
Email: re.roohi@gmail.com

splitter beam or plate attached to the cylinder and immersed in the fluid flow [10]. The beam vibrations are due to the formation and detachment of the vortices from the cylinder. The vortex street causes a pulsating force on the beam which in turn oscillates the beam and its oscillations affect the flow field. So, the vibrations of the beam downstream of the cylinder is a fluid-solid interaction (FSI) problem. Lee and You [11] studied the vortex-shedding-induced vibration of a splitter plate behind a cylinder. They obtained their results at a low Reynolds number and show that the plate deflection is dependent on the plate length. The vibrational behavior of a flexible splitter plate attached to a square cylinder in laminar flow in a vortex street is analyzed by Sun et al. [12]. Zhu et al. [13] numerically investigated the effect of upstream and downstream placement of circular cylinder with splitter plate on the flow characteristics and vibrational behavior of the beam. The dynamic behavior of two cantilevered flexible plates aligned parallel to each other in axial flow is investigated by Tang and Païdoussis [14]. Wong et al. [15] experimentally analyzed the dynamic response and wake structure of a rotating circular cylinder undergoing vortex-induced vibration for 1100<Re<6300. Zou et al. [16] numerically investigated the flow-induced vibration of a rotating cylinder and obtained that the Rotation increased the vibration of the cylinder in the flow direction and decreased the vibration in the crossflow direction. Hofstede et al. [17] simulated the flow-induced vibration of nuclear fuel rods in axial turbulent flows. The vortex-induced vibration of an asymmetrical composite beam bridge under five wind attack angles and two wind directions is studied by Wang et al.[18]. Their experimental results and simulations indicate that the properties of the vortex-induced vibrations vary with the wind direction; for example, the vertical maximum VIV amplitude of the bridge occurred at the wind attack angle of −5° and wind direction of 180°. Sahoo et al. [19] investigated the dynamic behavior of a beam and a wake oscillator model ascribing vortex-induced vibrations under high-frequency excitation.

The flow-induced vibration of a beam or plate can be used to extract electrical power by utilization of a piezoelectric beam in the structure or attach a piezoelectric device to the free end of the system [12, 20]. For the first time, Allen and Smits [21] examined the feasibility of placing a piezoelectric membrane in the wake of a bluff body. They determined that the maximum output power is obtained when the resonance condition occurs in the membrane. Shan et al. [22] analyzed an underwater energy harvester based on the flow-induced vibration. The effect of the Reynolds number on the vortex-induced vibration of a circular cylinder and the attached piezoelectric beam is performed by Zhang et al. [23]. Karimzadeh et al. [24] investigated a size-dependent micro energy harvester based on the VIV beam and attached piezoelectric layer. They studied the effect of length the scale parameter, load resistance and fluid velocity on the vibrational behavior and the produced power of the system.

As it is discussed above, the vibration frequency of VIV systems is a combination of vortex shedding frequency and splitter plate natural frequency [11], therefore the effect of flow parameters and geometric parameters of the splitter plate on the device frequency should be analyzed which is not performed properly in the literature. For this purpose in the present study, the FSI model of transient oscillations of a fixed cylinder attached to an elastic splitter plate is established to determine the splitter motion patterns and their effect on the vortex shedding and piezoelectric output power. The effect of several involving parameters including the inlet fluid velocity, splitter plate length and its stiffness on the obtained power is examined. Finally, some complementary comments regarding the applicability of the proposed configuration to harvest clean energy in realistic scenarios are mentioned.

Nomenclature

t	time
v_f	Fluid velocity in a fixed coordinate
p	pressure
μ	viscosity
v_r	Velocity vector relative to moving frame
I	Diagonal unit matrix
F_E	Forces in the Eulerian frame
F_L	Forces in the Lagrangian frame

σ	Second Piola-Kirchhoff stress tensor
Ψ	Fourth order elasticity
ε	Green-Lagrange strain
S	Cauchy stress

2. Mathematical modeling and governing equations

2. 1. Fluid-solid governing equation

The fluid-solid interaction problem of flexible beam vibrations is solved using the COMSOL solver based on the Arbitrary Lagrangian-Eulerian (ALE) method. According to this method, the fluid flow governing equations are solved using the spatial frame of reference (Eulerian approach), while the material reference frame (Lagrangian approach) is implemented to determine the transient deformation of the oscillating beam. To represent the governing equations, let's assume that the fluid, solid and their interface is denoted by Π_f, Π_s, and Θ, respectively.

The flow field is determined based on the assumption of unsteady, incompressible, Newtonian and laminar flow passing over an elastic object as [25]:

$$\nabla.v_f = 0 \tag{1}$$

$$\frac{\partial v_f}{\partial t} + \left(v_f - v_r\right).\nabla v_f = \nabla.\left[pI + \mu\left(\nabla v_f + \left(\nabla v_f\right)'\right)'\right], \quad \text{for } \Pi_f \tag{2}$$

where in the above equations, t, v_f, p and μ are time, fluid velocity in fixed coordinate, pressure and viscosity, respectively. v_r is the velocity vector relative to the moving reference frame and I is the diagonal unit matrix, in which the transpose operator is denoted by the ($'$) symbol. At the initial instance, both fluid velocity and pressure are set to zero. As different reference frames are applied for the fluid and solid equations, a transformation is needed to convert the hydrodynamic force between these two frames. That is

$$F_L = F_E.\left(dv/dV\right), \tag{3}$$

where dv, dV, F_E and F_L are sizing factors and forces in Eulerian and Lagrangian frames, respectively. Additionally, as the fluid domain deforms during the oscillations, the mesh motion and/or remeshing should be performed when necessary. The updated location of grid points can be determined using the solution of the Winslow equations for smoothing [26]. The new location of cell points is estimated by

$$\frac{\partial^2 \partial x_L}{\partial {x_E}^2 \partial t} + \frac{\partial^2 \partial x_L}{\partial {y_E}^2 \partial t} = 0, \tag{4}$$

$$\frac{\partial^2 \partial y_L}{\partial {x_E}^2 \partial t} + \frac{\partial^2 \partial y_L}{\partial {y_E}^2 \partial t} = 0 \tag{5}$$

The equations above are similar to the diffusion equation (due to the Laplacian nature of the Winslow equations). In these equations, the subscripts of E and L refer to the Eulerian and Lagrangian frames of reference. To determine the deformation of the splitter, the relation between the stress and strain tensors is utilized as

$$\left(\sigma - \sigma_0\right) = \Psi:\left(\varepsilon - \varepsilon_0\right), \quad \text{for } \Pi_s \tag{6}$$

where in the above equation, σ, Ψ and ε are the tensors of second Piola-Kirchhoff, fourth-order elasticity and Green-Lagrange strain, respectively. The magnitude of these tensors at the initial instances is determined by the '0' subscript and the double-dot product operator is represented by ':'. Based on the obtained values of the solid displacement (u_s), the Green-Lagrange strain tensor can be calculated as [27]

$$\varepsilon = \frac{1}{2}\left[\left(\nabla u_s\right)' + \nabla u_s + \left(\nabla u_s\right)'\nabla u_s\right], \quad \text{for } \Pi_s \tag{7}$$

Moreover, to determine the movement of the splitter surface points, the elastic behavior of the beam is utilized as [6]

$$\rho_s \frac{\partial^2 u_s}{\partial t^2} = \nabla.S + F_L, \quad \text{for } \Pi_s \tag{8}$$

where F_L as the force exerted by the fluid and S known as Cauchy stress and is determined as [28]

$$S = \frac{1}{\det\left(I + \nabla u_s\right)}\left(I + \nabla u_s\right)\sigma\left(I + \nabla u_s\right)', \quad \text{for } \Pi_s \tag{9}$$

For the initial and boundary conditions for the solid displacement equation, it is assumed that the system is at rest (zero displacements and velocity) at the initial state, and the boundary cells at the cylinder surface are assumed to be fixed.

Additionally, at the fluid-solid interface, the displacement and force should be balanced at both fluid and solid sides. So, the following

equations (Eq. 10 for geometry and Eq. 11 for force) should be satisfied:

$$v_f = \frac{\partial u_s}{\partial t} \quad \text{for } \Theta \tag{10}$$

$$\left(-pI + \mu\left(\nabla v_f + \left(\nabla v_f\right)^t\right)\right).n_f + S.n_s = 0 \tag{11}$$

where n_f and n_s are the unit vectors normal to the interface boundary.

2. 2. Solution method:

To solve the flow governing equations the collocated (non-staggered) method with a second-order central difference for spatial derivatives, as well as fractional time-step for the unsteady term, is implemented. The fractional time step consists of two subsequent parts for the advection-diffusion equation as well as the Poisson's equation for pressure estimation. To ensure the solution convergence at each time step several iterations are performed until the interface convergence criteria (compatibility of fluid force and structure deflection at the interface) is achieved.

The time step is dependent on the frequency of the oscillations, so based on the time step independency test, a time step equal to 0.001 s is selected and applied to all of the examined cases. The simulation is performed on a computational system equipped with Intel® Core™ i7 CPU (3.5GHz for each core), 16 GB physical memory and ATI Radeon™ 6490M 256 GB GPU.

2. 3. Problem description:

Self-inducted vibrations of a flexible splitter plate attached to a cylinder is numerically simulated. The flow and deformation fields are determined based on the solution of a set of non-linear coupled equations. To prevent the effect of flow blockage on the obtained results, the computational domain is extended to 10 D and 30 D in height and width. For the fluid-solid interfaces, the no-slip boundary condition is assigned which denotes the zero velocity at the fixed wall faces, while at the moving boundaries, the compatibility of the solid and fluid domains is applied.

For the left face, the uniform velocity inlet boundary condition is assigned based on the magnitude of the examined *Re*. At the upper and lower faces, two types of boundary conditions are set. For the validation with experimental data, as the fluid flow through a duct is modeled, these boundaries are set to no-slip condition. For the rest of the numerical simulation, the vibrations are assumed to occur at the free stream of the fluid and consequently, the open boundary condition is assigned. As the simulated system has a high aspect ratio and the blockage effect is negligible, the pressure field at the upper and lower boundaries are not affected and the open boundary condition is valid.

Moreover, the right surface is set as the pressure constant face at the atmospheric pressure. For the structural deformation, the fixed B.C. at the cylinder face as well as the hydrodynamic force at the splitter surface is assigned. The hydrodynamic force is affected by both fluid shear and pressure stresses which are estimated based on the flow field calculations at each computational time step.

To introduce the non-dimensional parameter groups, the cylinder diameter and far-field velocity are chosen as the non-dimensionalization scales. So the following dimensionless variables are introduced and used in the following discussions:

$$Re = \frac{\rho_f^* u_m^* D^*}{\mu^*} \qquad E = \frac{E^*}{\rho_f^* u_m^{*2}} \qquad \rho_s = \frac{\rho_s^*}{\rho_f^*}$$

$$St = \frac{f_s D}{U_\infty} \qquad C_L = \frac{F_L}{0.5\rho U_\infty^2 D} \qquad C_P = \frac{P - P_\infty}{0.5\rho U_\infty^2} \tag{12}$$

$$C_D = \frac{F_D}{0.5\rho U_\infty^2 D}$$

The utilized computational domain is illustrated in Fig. 1. To obtain accurate numerical results several considerations are accounted for in the meshing procedure. Three main schemes are utilized for different parts of the domain. For the solid domain (including the fixed cylinder and

the deformable plate) a triangular distribution of the cells is implemented. The cells are uniformly distributed within the solid region, however, the density number is higher near the tip of the plate. For the fluid zone in the remeshing part (*i.e.* the left zone including the oscillator), the boundary layer near the solid walls with five layers of gradually increasing height is utilized. As the remeshing procedure is applied, the grid density near the regions with higher deformation (i.e. at the end of the plate) is increased. The growth ratio of the cells from small to large cells is set to 1.1 to prevent sharp variations in the cells' sizing.

For the undeformed region (*i.e.* the right rectangular zone), a structured distribution of rectangular cells is assigned. The size of the cells is set to increase gradually from the interface surface with the left zone to the outlet boundary condition at the right side of the domain. To determine the sufficiency of the size of the implemented grid cells, the grid independency test is utilized. To do so, the four different computational cells with identical meshing schemes at various cell numbers are applied and the tip deflection is observed as the decision parameter. The number of the grid cells are 35451, 51975, 73555 and 97743.

The simulated geometry is revealed in Fig 2, which includes the fixed cylinder, the vibrating plate, the moving mesh region and the fixed zone. As the oscillations of the plate affect the distribution of the computational grids, at each time step, it is necessary to update the grids. However, as the remeshing process is time-consuming and a large portion of the utilized mesh is unaffected by the vibrations of the beam, the domain is divided into two regions for remeshing in the vicinity of the system and fixed at farther regions.

3. Results and discussion

In order to investigate the accuracy of the present simulations, a flow past over a deformable plate attached to a circular cylinder similar to [11] and [6] is considered and the results are presented in Fig. 3. In this figure the Reynolds number based on the cylinder diameter D and the mean fluid velocity is assumed to be 200. The dimensionless physical parameters for this test are the ratio of structural density to fluid density ($\rho_s = 10$), dimensionless Young's modulus ($E = 1400$) and Poisson's ratio ($\nu = 0.4$) and the time step is set to $\Delta t = 0.005$. Findings indicate that the present solution is in complete agreement with previous theoretical research [6] and the maximum computed error with the experimental study [11] is under 8%.

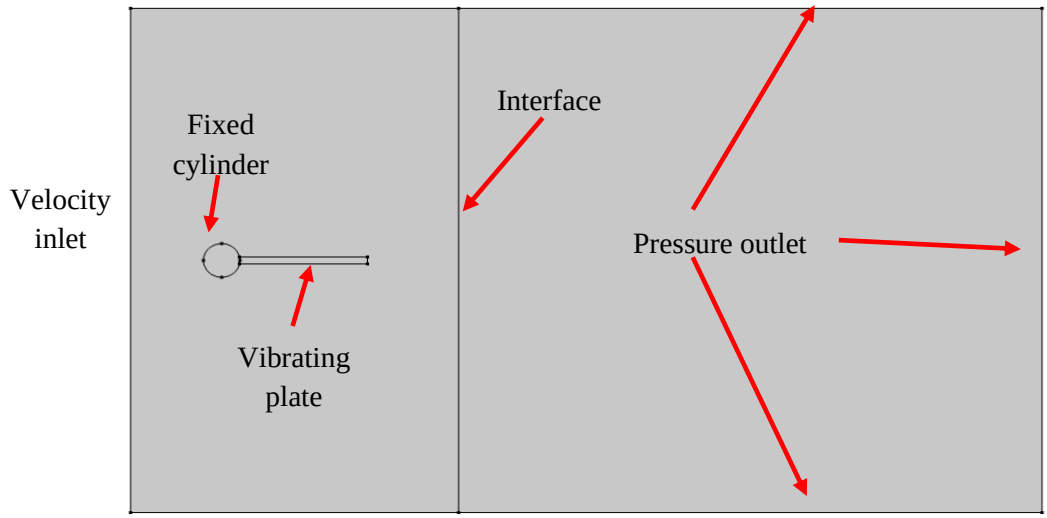

Fig. 1. The representation of the computational domain as well as the assigned boundary conditions.

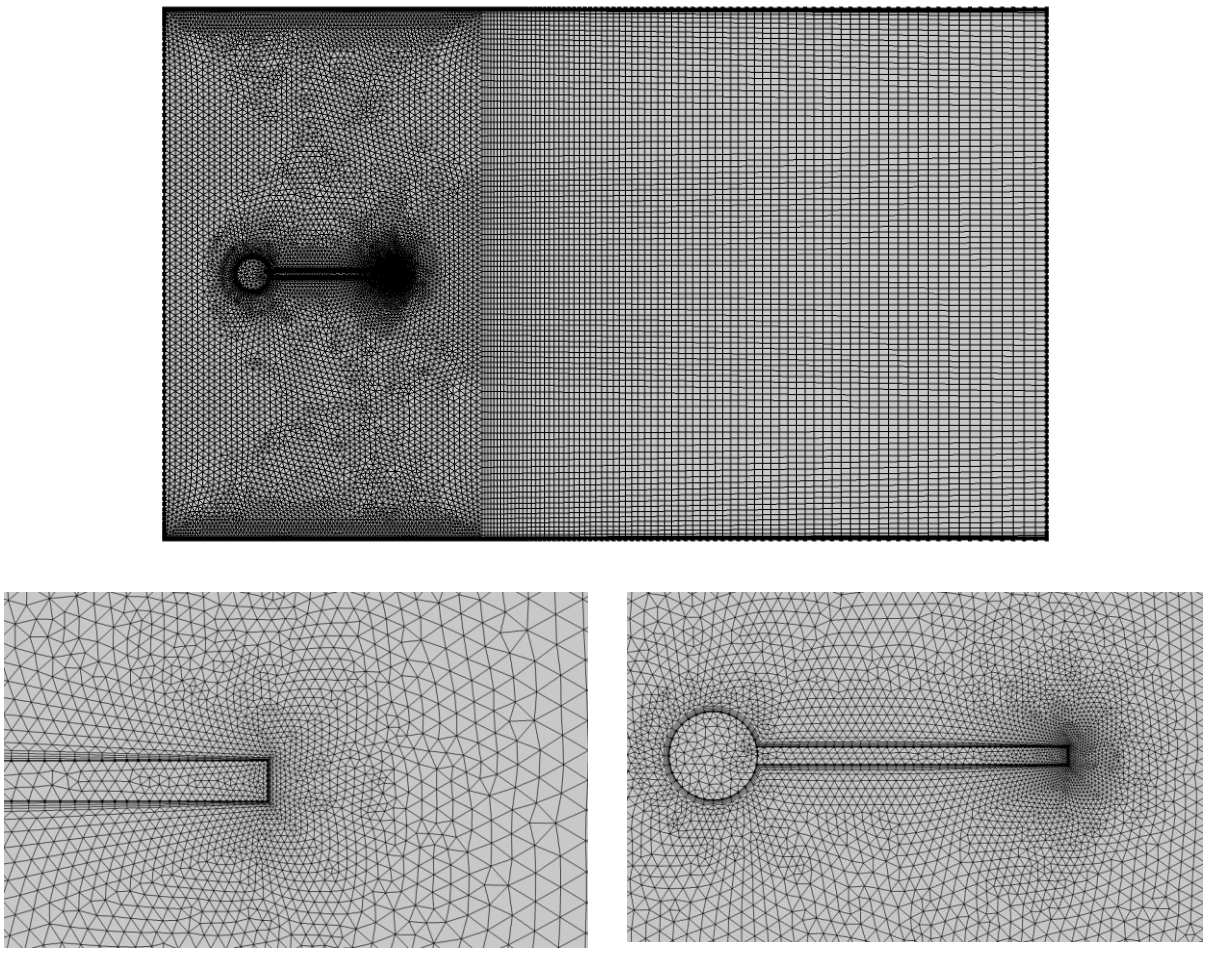

Fig. 2. View of the fluid mesh near a circular cylinder attached to a flexible plate.

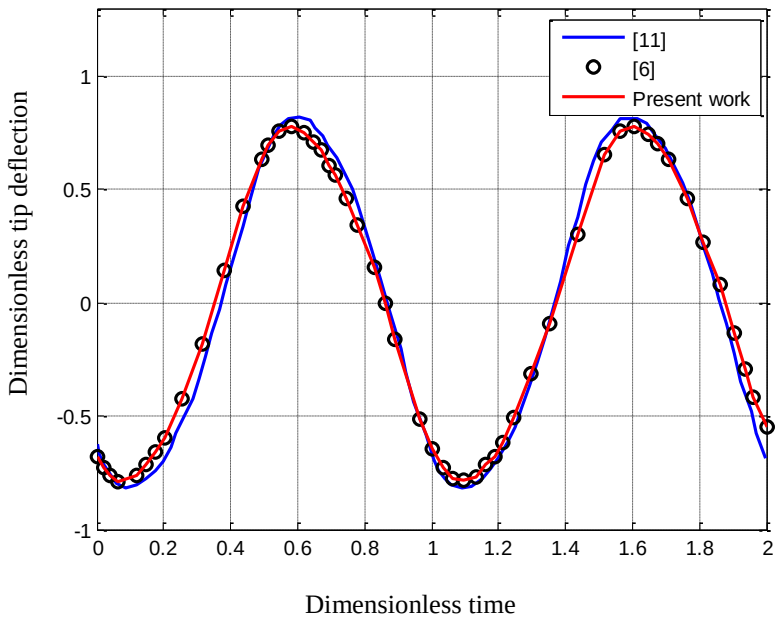

Fig. 3. Time histories of the dimensionless vertical displacements of the plate tip.

The vorticity contours and structural deformations at four equally spaced time points in one period of oscillations for the main analyzed structure ($L = 1, U = 1, E = 10000$) and various dimensionless parameters such as Young modulus ($E = 2500, 40000$), plate length ($L = 0.25, 4$), and fluid velocity ($U = 16$) is obtained and illustrated in Fig. 4. Outcomes indicate that for $E = 2500$ the plate is more flexible than the main structure and the plate deflection is increased but for $E = 40000$ the plate is stiffer and no vibration occurs in the plate. Increasing the beam length from $L = 0.25$ to 1 and 4 decreases the plate stiffness and the vibration in the beam is more visible. These results can be explained according to the splitter plate's natural frequency, where the plate frequency is proportional to E and $\frac{1}{L}$, increasing the length and decreasing the Young modulus will decrease the natural frequency, and therefore oscillation in the structure and lock-in phenomena occurs at lower fluid velocities. Results also reveal that the vortex shedding frequency is only dependent on the fluid velocity and Reynolds number and other investigated parameters have no effect on the vortices frequency. The vortex shedding is due to the instability that occurred in the wake region of the fixed cylinder and its interaction with the motion of the vibrating plate.

The effect of dimensionless Young modulus on the dynamic response of the system is illustrated in Fig. 5. As it is seen, reduction in E at constant fluid velocity decreases the stiffness of the system and at specified vortex frequency, higher mode shapes of the plate are excited and respectively higher oscillations and output power can be obtained from the device. For the stiffer plate ($E = 40000$), only the first mode shape with low vibration amplitude is observed therefore the estimated extracted power would be lower than the softer plate ($E = 2500$).

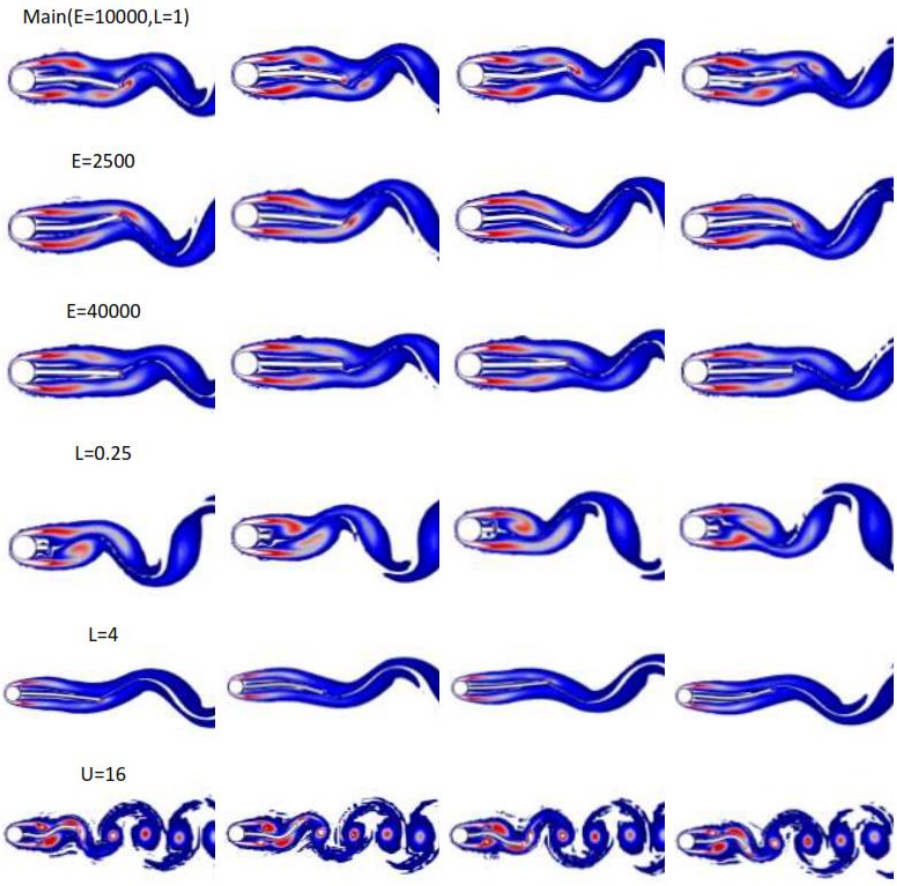

Fig. 4. Vorticity contours and structural deformations at four selected time points.

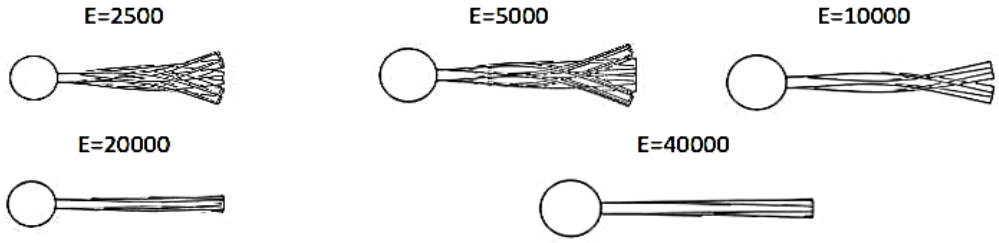

Fig. 5. Variation of the superimposed view of the plate vibration mode versus dimensionless Young modulus at Re=200.

In Fig.6 the superimposed mode shapes of the plate for different lengths are plotted. According to the literature [29], the natural frequency and corresponding mode shapes of a plate are proportional to $\frac{1}{L}$. Present findings reveal that by increasing the dimensionless length from 0.25 to 4 the natural frequencies of the plate are decreased and more mode shapes and corresponding natural frequencies are excited and observed in the response of the system. For example, for L=0.25 no vibration is detected and none of the modes is excited, for L=0.5 and L=1 only the first mode is excited while for L=2 and L=4, the second and third modes with higher deflection are obviously excited. This phenomenon gives that increasing the beam length reduces the beam's natural frequency and changes the vortex-shedding frequency of the VIV device. It can be concluded that the equality of plate natural frequency and vortex shedding frequency (lock-in phenomena) for devices with higher plate lengths happens at lower fluid velocities.

The effect of the dimensionless density ratio on the excited mode of the system is presented in Fig. 7. For $\rho_s = 2.5$ to 20 only the first mode of the plate is excited and increasing the dimensionless density has no effect on the device behavior, while for $\rho_s = 40$ the second mode of the structure is observed in the dynamic response. This behavior can be explained by the dimensionless Young modulus where for a constant E^* and fluid velocity, increasing the density ratio of the solid to fluid decreases the stiffness of the system, and therefore, higher mode shapes and the corresponding natural frequencies are excited and play a substantial role in the vibrational behavior of the structure.

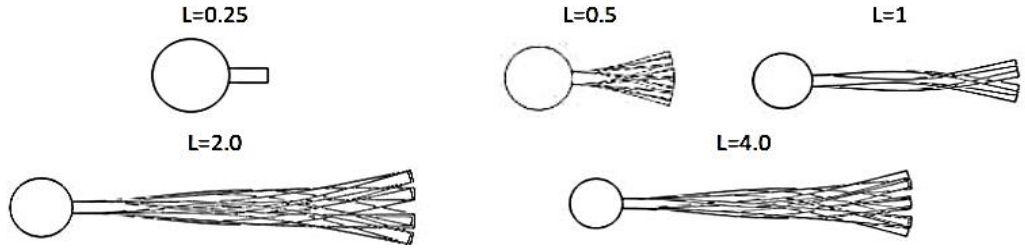

Fig. 6. Variation of the superimposed view of the plate vibration mode versus plate length at Re=200.

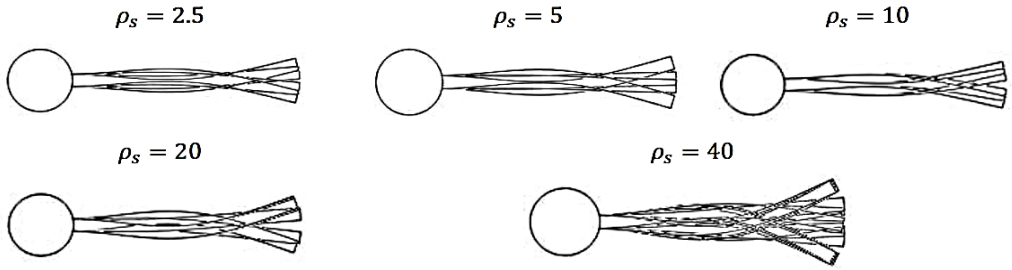

Fig. 7. Variation of the superimposed view of the plate vibration mode versus dimensionless density at Re=200.

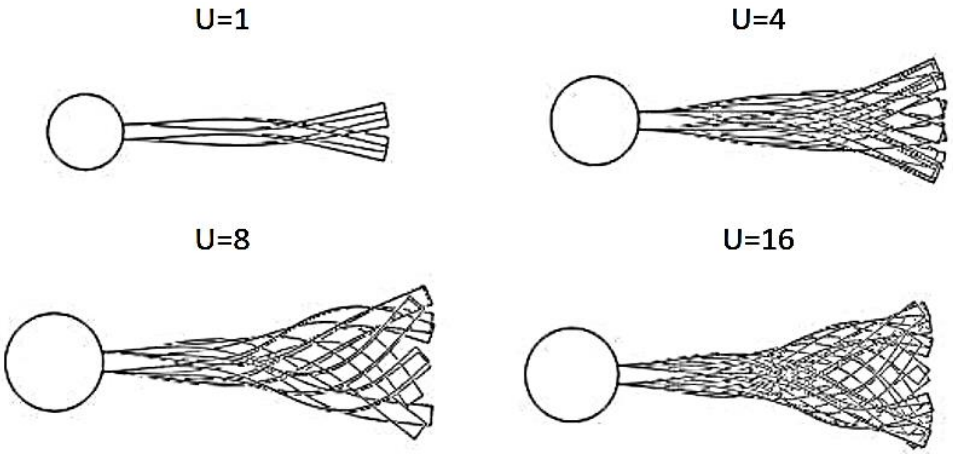

Fig. 8. Variation of the superimposed view of the plate vibration mode versus fluid velocity at Re=200.

In the study of vortex-induced vibration of the plate, fluid velocity plays an important role in the dynamic response of the solid structure and the obtained output power. This behavior is clearly illustrated in Fig. 8. As it is depicted in this figure, for the fluid velocity 1, 4, 8 and 16, the 1st, 1st and 2nd, first three and first four mode shapes are excited respectively and higher plate deflections are obtained. This observation reveals that in analytical analysis of these systems based on the mode of the system sufficient mode shapes of the plate must be considered to obtain precise results. In addition to that, increasing the fluid velocity increases the vortex shedding frequency, and therefore higher mode shapes and corresponding natural frequencies are excited.

4. Conclusion

In order to investigate the combined effect of vortex shedding frequency and splitter plate natural frequency on the vibrational behavior of VIV systems, in the present work the transient vibration of a fixed cylinder attached to an elastic piezoelectric splitter plate in a flow field is studied. For the described problem, the FSI model is developed to obtain the splitter motion patterns and the effect of that on the vortex shedding and predicted output power. The effect of parameters such as the inlet fluid velocity, density ratio (ratio of solid density over fluid density), splitter plate length and young modulus of elasticity on the vibrational response of the device is examined. The outcomes of the present study are compared with the theoretical and experimental results reported in the literature and great agreement is observed. Findings show that decreasing dimensionless plate Young modulus or increasing dimensionless plate length decreases the natural frequency of the system and higher modes of the device take part in the dynamic behavior of the system. In addition to that, by increasing the fluid velocity from 1 to 4, 8 and 16, respectively the excitation modes of 1st, 1st and 2nd, first three and first four are activated and higher plate deflections are obtained. This observation reveals that for precise analysis of these systems, sufficient mode shapes of the plate must be considered.

References

[1] Z. Wu, J. Wang, Y. Liu, S. Hou, X. Liu, Q. Zhang, et al., "A review of spectral controlling for renewable energy harvesting and conserving," Materials Today Physics, vol. 18, p. 100388, 2021.

[2] S. P. Madhusudanan, S. C. Caroline, and S. K. Batabyal, "Sustainable energy harvesting technologies," in Sulfide and Selenide Based Materials for Emerging Applications, ed: Elsevier, 2022, pp. 15-33.

[3] S. Wang, W. Liao, Z. Zhang, Y. Liao, M. Yan, and J. Kan, "Development of a novel non-contact piezoelectric wind energy harvester excited by vortex-induced vibration," Energy Conversion and Management, vol. 235, p. 113980, 2021.

[4] Z. Esa, J. H. Zaini, M. Mehdi, A. Iqbal, and M. M. Nauman, "Design, Fabrication & Analysis of a Gravitational Water Vortex

Based Energy Harvester," International Journal of Green Energy, pp. 1-12, 2022.
[5] Q. Wen, X. He, Z. Lu, R. Streiter, and T. Otto, "A comprehensive review of miniatured wind energy harvesters," Nano Materials Science, vol. 3, pp. 170-185, 2021.
[6] H. Wang, Q. Zhai, and J. Zhang, "Numerical study of flow-induced vibration of a flexible plate behind a circular cylinder," Ocean Engineering, vol. 163, pp. 419-430, 2018.
[7] N. Wu, B. Bao, and Q. Wang, "Review on engineering structural designs for efficient piezoelectric energy harvesting to obtain high power output," Engineering Structures, vol. 235, p. 112068, 2021.
[8] J. Wang, L. Geng, L. Ding, H. Zhu, and D. Yurchenko, "The state-of-the-art review on energy harvesting from flow-induced vibrations," Applied Energy, vol. 267, p. 114902, 2020.
[9] X. Ma and S. Zhou, "A review of flow-induced vibration energy harvesters," Energy Conversion and Management, vol. 254, p. 115223, 2022.
[10] G.-P. Cui and L.-H. Feng, "Suppression of vortex-induced vibration of a circular cylinder by a finite-span flexible splitter plate," Physical Review Fluids, vol. 7, p. 024708, 2022.
[11] J. Lee and D. You, "Study of vortex-shedding-induced vibration of a flexible splitter plate behind a cylinder," Physics of Fluids, vol. 25, p. 110811, 2013.
[12] X. Sun, C. S. Suh, C. Sun, and B. Yu, "Vortex-induced vibration of a flexible splitter plate attached to a square cylinder in laminar flow," Journal of Fluids and Structures, vol. 101, p. 103206, 2021.
[13] H. Zhu, G. Li, and J. Wang, "Flow-induced vibration of a circular cylinder with splitter plates placed upstream and downstream individually and simultaneously," Applied Ocean Research, vol. 97, p. 102084, 2020.
[14] L. Tang and M. P. Païdoussis, "The coupled dynamics of two cantilevered flexible plates in axial flow," Journal of Sound and Vibration, vol. 323, pp. 790-801, 2009.
[15] K. W. L. Wong, J. Zhao, D. L. Jacono, M. C. Thompson, and J. Sheridan, "Experimental investigation of flow-induced vibration of a sinusoidally rotating circular cylinder," Journal of Fluid Mechanics, vol. 848, pp. 430-466, 2018.
[16] Q. Zou, L. Ding, H. Wang, J. Wang, and L. Zhang, "Two-degree-of-freedom flow-induced vibration of a rotating circular cylinder," Ocean Engineering, vol. 191, p. 106505, 2019.
[17] E. Ter Hofstede, S. Kottapalli, and A. Shams, "Numerical prediction of flow induced vibrations in nuclear reactor applications," Nuclear Engineering and Design, vol. 319, pp. 81-90, 2017.
[18] J. X. Wang, C. M. Ma, M. Li, N. Yeung, and S. Li, "Experimental and numerical studies of the vortex-induced vibration behavior of an asymmetrical composite beam bridge," Advances in Structural Engineering, vol. 22, pp. 2236-2249, 2019.
[19] P. K. Sahoo and S. Chatterjee, "Nonlinear dynamics of vortex-induced vibration of a nonlinear beam under high-frequency excitation," International Journal of Non-Linear Mechanics, vol. 129, p. 103656, 2021.
[20] G.-P. Cui, L.-H. Feng, and Y.-W. Hu, "Flow-induced vibration control of a circular cylinder by using flexible and rigid splitter plates," Ocean Engineering, vol. 249, p. 110939, 2022.
[21] J. J. Allen and A. J. Smits, "Energy harvesting eel," Journal of fluids and structures, vol. 15, pp. 629-640, 2001.
[22] X. Shan, H. Li, Y. Yang, J. Feng, Y. Wang, and T. Xie, "Enhancing the performance of an underwater piezoelectric energy harvester based on flow-induced vibration," Energy, vol. 172, pp. 134-140, 2019.
[23] M. Zhang, C. Zhang, A. Abdelkefi, H. Yu, O. Gaidai, X. Qin, et al., "Piezoelectric energy harvesting from vortex-induced vibration of a circular cylinder: effect of Reynolds number," Ocean Engineering, vol. 235, p. 109378, 2021.
[24] A. Karimzadeh, R. Roohi, and M. Akbari, "Size-dependent behavior of micro piezoelectric VIV energy harvester: Parametric study and performance

analysis," Applied Ocean Research, vol. 127, p. 103296, 2022.
[25] J. Donea, S. Giuliani, and J.-P. Halleux, "An arbitrary Lagrangian-Eulerian finite element method for transient dynamic fluid-structure interactions," Computer methods in applied mechanics and engineering, vol. 33, pp. 689-723, 1982.
[26] M. Y. Chong, B. Gu, B. T. Chan, Z. C. Ong, X. Y. Xu, and E. Lim, "Effect of intimal flap motion on flow in acute type B aortic dissection by using fluid-structure interaction," International journal for numerical methods in biomedical engineering, vol. 36, p. e3399, 2020.
[27] D. Jung and H. C. Gea, "Topology optimization of nonlinear structures," Finite Elements in Analysis and Design, vol. 40, pp. 1417-1427, 2004.
[28] W. M. Lai, D. H. Rubin, D. Rubin, and E. Krempl, Introduction to continuum mechanics: Butterworth-Heinemann, 2009.
[29] S. S. Rao, Vibration of continuous systems: John Wiley & Sons, 2019.